Article

Kinetics and Coverage Dependent Reaction Mechanisms of the Copper Atomic Layer Deposition from Copper Dimethylamino-2-propoxide and Diethylzinc

Yasheng Maimaiti, and Simon D Elliott

Chem. Mater., **Just Accepted Manuscript** • DOI: 10.1021/acs.chemmater.6b02522 • Publication Date (Web): 11 Aug 2016

Kinetics and Coverage Dependent Reaction Mechanisms of the Copper Atomic Layer Deposition from Copper Dimethylamino-2-propoxide and Diethylzinc

*Yasheng Maimaiti and Simon D. Elliott**

Tyndall National Institute, University College Cork, Lee Maltings, Prospect Row, Cork, Ireland

ABSTRACT: Atomic layer deposition (ALD) has been recognized as a promising method to deposit conformal and uniform thin film of copper for future electronic devices. However, many aspects of the reaction mechanism and the surface chemistry of copper ALD remain unclear. In this paper, we employ plane wave density functional theory (DFT) to study the transmetalation ALD reaction of copper dimethylamino-2-propoxide [$Cu(dmap)_2$] and diethylzinc [Et_2Zn] that was realized experimentally by Lee *et al.* [Angew. Chemie Int. Ed. **2009**, 48, 4536–4539]. We find that the $Cu(dmap)_2$ molecule adsorbs and dissociates through the scission of one or two Cu – O bonds into surface-bound dmap and Cu(dmap) fragments during the copper pulse. As Et_2Zn adsorbs on the surface covered with Cu(dmap) and dmap fragments, butane formation and desorption was found to be facilitated by the surrounding ligands, which leads to one reaction mechanism, while the migration of ethyl groups to the surface leads to another reaction

mechanism. During both reaction mechanisms, ligand diffusion and reordering are generally endothermic processes, which may result in residual ligands blocking the surface sites at the end of the Et_2Zn pulse, and in residual Zn being reduced and incorporated as an impurity. We also find that the nearby ligands play a cooperative role in lowering the activation energy for formation and desorption of by-products, which explains the advantage of using organometallic precursors and reducing agents in Cu ALD. The ALD growth rate estimated for the mechanism is consistent with the experimental value of 0.2 Å/cycle. The proposed reaction mechanisms provide insight into ALD processes for copper and other transition metals.

1. Introduction

The interest in depositing uniform and island-free ultrathin films of copper originates from its application as the interconnect material in electronic devices. Copper has superior properties to aluminium as an interconnect material, such as lower resistivity and higher current density for electromigration, which are critical for improved device performance and reliability.[1] Deposition techniques such as physical vapor deposition (PVD),[2] electrodeposition,[3] chemical vapor deposition (CVD)[4] and atomic layer deposition (ALD)[5–8] have been applied with the aim of obtaining a thin film of Cu. It is extremely difficult to deposit continuous thin films of Cu at 2 nm thickness and instead formation of Cu islands with size of 10-90 nm tends to be more favourable.[9] Of these deposition approaches, ALD shows the most promise in surmounting the island growth problem as well as meeting future demands of device scaling.[10–12]

Many copper organometallic compounds are used with H_2 or H_2 plasma in copper ALD experiments[13–18]. However, these processes lead to impurities and discontinuous films either because of the higher temperature requirement or because of the strong reducing or oxidizing nature of the co-reagents.[8,19,20] Significant progress was made by Lee *et al.* in developing low

temperature ALD of copper metal using the reaction of copper dimethylamino-2-propoxide [$Cu(dmap)_2$] and diethylzinc [Et_2Zn] at 100–120 °C.[21] Although subsequent work reported that the parasitic CVD reaction of Et_2Zn may lead to Zn incorporation into the copper thin film,[20] the work by Lee *et al.* has important implications on the co-reagent strategy which was traditionally limited to the use of molecular or plasma H_2. The reaction of $Cu(dmap)_2$ and Et_2Zn was previously used to synthesize Cu/Zn alloy nanocolloids using thermolysis.[22] Vidjayacoumar *et al.* investigated ALD reactions of eight different copper (II) complexes separately with $AlMe_3$, BEt_3 and Et_2Zn in order to identify the most promising combination of the copper precursor and co-reagent.[20,23] The reductive properties of various metallocenes along with different copper precursors were investigated with density functional theory (DFT) and solution phase chemistry to evaluate the use of metallocene compounds as reducing agents for Cu ALD.[24]

$Cu(dmap)_2$ has been a popular choice for other Cu ALD processes. For example, Knisley *et al.* reported a low temperature three-step ALD process using $Cu(dmap)_2$, formic acid (HCO_2H) and hydrazine (N_2H_4) at 120 °C and indicated that their method can avoid undesired elements in the precursors and affords high purity low resistivity copper metal.[6] Kalutarage *et al.* compared two-step and three-step processes using the ALD reaction of $Cu(dmap)_2$ with $BH_3(NHMe_2)$ and separately with $BH_3(NHMe_2)$ and HCO_2H.[9] They showed that the two-step process requires a Cu seed layer, and affords a growth rate of about 0.13 Å/cycle within the 130−160 °C ALD window. The three-step process does not need a Cu seed layer for growth, and affords a growth rate of 0.20 Å/cycle within the 135−165 °C ALD window. Guo *et al.* explored an ALD process for depositing copper thin film on silicon wafers and glass slides at 50 °C using copper(I)-N,N′-diisopropylacetamidinate precursor and H_2 plasma.[25] The focus in many of those experimental works is on the deposition and characterization of copper thin films, with less elaboration of the

self-terminating surface reactions that are important requirement for an ALD process. Computational studies such as electronic structure calculations can be an efficient way to investigate the surface reactions during ALD and provide useful information to develop better processes.[26] For instance, developing a model for island formation will require knowledge of the kinetics of the underlying deposition reactions.

Although the ALD mechanisms of metal oxides are well understood,[27–29] very few theoretical[30–32] and *in situ* experimental[33,34] works have been dedicated to understand the reaction mechanisms of copper and related metals. Dey *et al.* used a gas phase model to study the reactions of several common Cu precursors with Et_2Zn.[30] Copper(I) carbene hydride complexes which act both as reducing agent and precursor for Cu ALD were proposed by Dey *et al.* in a gas phase density functional theory (DFT) study.[35] However, since ALD is based on self-terminating surface reactions, it is necessary to understand the role of the surface. Dey *et al.* also investigated the surface reactions of several copper precursors and diethylzinc to identify an effective ALD process.[36] They found that dmap-type ligands are best for ALD of copper while the reducing agent Et_2Zn is not a good choice because it dissociates into ZnEt and Et fragments on a bare copper surface, which may result in the Zn impurity observed in experimental work. Hu *et al.* compared the adsorption of $(^nBu_3P)_2Cu(acac)$ and $Cu(acac)_2$ precursors on Ta(110) surface using DFT calculations and found that the $(^nBu_3P)_2Cu(acac)$ precursor prefers to dissociate in the gas phase while $Cu(acac)_2$ favours decomposition on the Ta surface.[37] Recently, Hu *et al.* studied the surface chemistry of copper metal and copper oxide ALD from copper(II) acetylacetonate [$Cu(acac)_2$] and different co-reagents (e.g. H_2, atomic H and H_2O) using periodic DFT and reactive molecular dynamics.[38] Ma *et al.* found that the ligands of $Cu(acac)_2$ decompose when they adsorb onto bare Cu.[39]

In a previous publication, we explained how ALD deposited copper oxide thin films can be reduced to metallic copper through oxygen vacancy formation and H_2 adsorption.[40] Previously, we also studied the adsorption of $Cu(dmap)_2$ on flat and rough copper surfaces using DFT with different treatments of van der Waals (vdW) interaction.[41,42] We found that the adsorption energies and geometries of the $Cu(dmap)_2$ adsorbed on the Cu surfaces depend substantially on the adsorption sites and treatment of vdW interactions. Based on this in-depth investigation of the precursor, we now proceed to study the full ALD reaction cycle using $Cu(dmap)_2$ and the Et_2Zn co-reagent.

In their original work, Lee *et al* proposed a transmetalation reaction of $Cu(dmap)_2$ and Et_2Zn, which yields metallic copper and by-products $Zn(dmap)_2$ and butane as shown in Equation (1):

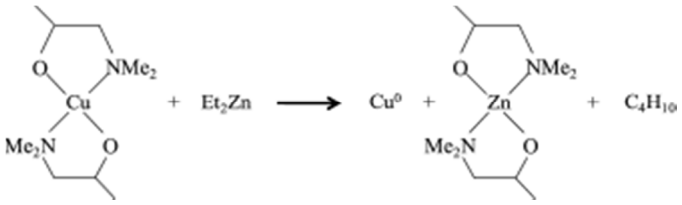

(1)

Because the ALD mechanism of the reaction in Equation (1) is not clear, we compare the reaction mechanisms of Al_2O_3 ALD and its analogy for Cu ALD, which are shown in Figure 1. Al_2O_3 ALD is a well-known model system for explaining ALD in general.[27,43,44] The Al_2O_3 ALD growth consists of alternating exposure of trimethylaluminum (TMA) and H_2O (Figure 1a). Note that the partition of each pulse into two steps (a, b) is conceptual. Each step may be self-limiting – i.e. there are two ways to achieve self-limiting ALD. During the first pulse, TMA reacts with the hydroxyl groups on the substrate to deposit Al_2O_3 and form CH_4 by-product (step 1a). Even when all hydroxyl groups have reacted, TMA continues to adsorb on the newly formed Al_2O_3 surface until the surface is fully saturated with CH_3 groups (step 1b). Notice that s-Al(CH_3)

represents any TMA fragments, *e.g.* $Al(CH_3)_2$. During the water pulse, H_2O reacts with the $Al(CH_3)$ covered surface to form Al_2O_3 (step 2a). Further adsorption of H_2O on the Al_2O_3 surface results in the surface saturated with OH groups (step 2b), which completes a full reaction cycle.

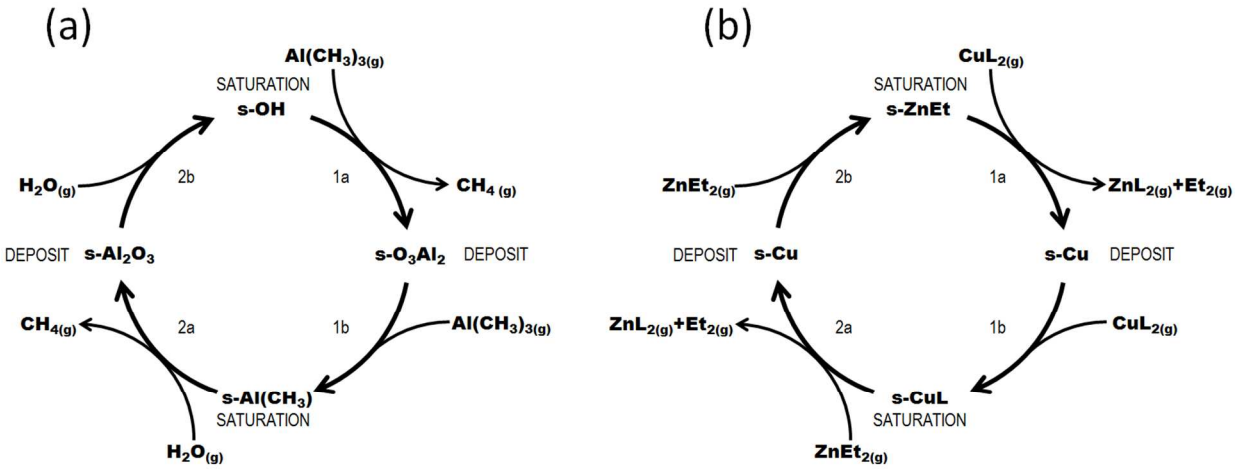

Figure 1. Schematic illustrations of (a) the known Al_2O_3 ALD mechanism and (b) Cu ALD from Equation 1. Surface species are labelled with 's-' and 'L' represents the dmap ligand in (b).

In Figure 1a, the Al_2O_3 ALD mechanism is represented with separate ligand elimination and ligand saturation steps in each cycle. Applying the same representation to the ALD of Cu, it is possible to propose a cyclic process for the reaction between CuL_2 (L=dmap) and Et_2Zn, as shown in Figure 1b. During the copper pulse, it is proposed in Eq. 1 that the CuL_2 reacts with the ZnEt covered surface to form metallic copper and gives by-products of ZnL_2 and butane (step 1a). The CuL_2 decomposes on the surface to form CuL covered surfaces (step 1b). As Et_2Zn is admitted in step 2a, direct analogy with the oxide ALD would in fact give Zn impurity as the deposited product and dmap-Et as by-product. However, Eq. 1 instead proposes that Cu is deposited by transmetalation and the Zn is etched away as ZnL_2, as shown in Figure 1b. The success of transmetalation is based on the Cu compound decomposing into butane + Cu.

Therefore, in the Zn pulse, adsorption of Et_2Zn (step 2a) leads to the same reaction as step 1a. In step 2b, the further adsorbed Et_2Zn decomposes on the bare Cu surface to form a ZnEt covered surface, ready for the next cycle.

Having postulated this reaction cycle, it is interesting to ask whether each step is thermodynamically favourable and kinetically viable, but also whether each step self-limits as required for ALD, or whether competing reactions play an important role. We would also like to estimate the ALD growth rate for this reaction cycle and compare it with experiment. The amount of Cu deposited in each cycle will be limited by the saturating coverage of Et ligands (prior to step 1a) and the saturating coverage of dmap ligands (at the end of step 1b). However, if surface diffusion of Et or dmap ligands is slow, then a saturating coverage may not be achieved and the process will instead be limited by the availability of adsorption sites for $Cu(dmap)_2$ during these steps.

In this work, we use the periodic DFT method to investigate the kinetics and reaction mechanism of the Cu ALD proposed in Figure 1b. To this end, we calculate the activation barriers (E_a) and reaction energies (ΔE) of a series of surface reactions to study the reaction pathways and energetics for a full cycle of the surface reaction of $Cu(dmap)_2$ and Et_2Zn in Equation (1). We will start the process with step 1b, namely the adsorption and decomposition of $Cu(dmap)_2$ precursor on bare Cu surfaces. We show that the $Cu(dmap)_2$ dissociates, through the scission of Cu – O bonds and produces dmap and Cu(dmap) fragments that saturate the surface in the first pulse. Butane formation with the assistance of ligands and the diffusion of ethyl groups on the surface can lead to different reaction mechanisms during the steps when ligands mix on the surface (step 2a of the Et_2Zn pulse and step 1a of the CuL_2 pulse), because of the different surface coverage of dmap ligands. We demonstrate that the activation energies for the

formation and desorption of Et_2Zn and $Zn(dmap)_2$ by-products are lowered by nearby ligands, which explains the advantage of using organometallic precursors and reducing agents in Cu ALD. The proposed ALD mechanisms provide insight into how to achieve the ALD of copper and other transition metals.

2. Computational Method

All calculations were performed using the Vienna Ab Initio Simulation Package (VASP 5.3).[45,46] Projector augmented wave (PAW)[47] potentials were used to represent the effective core electrons and nuclei. Electronic optimization was performed self-consistently using the plane wave basis set with a cutoff energy of 450 eV for the valence electrons. The Perdew−Burke−Ernzerhof (PBE)[48] functional was used to describe exchange and correlation effects. The impact of vdW forces on activation barriers and reaction energies is also assessed for some cases using vdW-optB88[49,50] and the choice of vdW-optB88 is justified in Ref [41]. The effect of spin polarization was found to be negligible for tests on the activation and reaction energies and thus non-spin-polarized calculations were performed. It was also found to be adequate to use only the Γ point to sample the Brillouin zone for all the calculations because of the large cell sizes. The adsorption of $Cu(dmap)_2$ on the Cu(111) surface with the four layered (6.289 Å thick) slabs separated by 18 Å of vacuum was tested on three different supercells: p(4 × 4), p(5 × 5) and p(6 × 6). It is found that the $Cu(dmap)_2$ does not adsorb on p(4 × 4) - Cu(111) surface. Although $Cu(dmap)_2$ chemisorbs on the bridge site on the Cu(111) surface with (5 × 5) expansion, the p(6 × 6) supercell was chosen for this study so as to have space for Et2Zn to adsorb as well. The simulation of one $Cu(dmap)_2$ and/or Et_2Zn within this supercell corresponds to a coverage of one molecule per surface area of 2.0 nm^2 (cell volume = 4.99 nm^3), following

our previous study in Ref [41]. A free area of about 2.0 nm^2 of bare Cu is thus required for molecular chemisorption of $Cu(dmap)_2$. The electronic energy convergence criterion is 10^{-4} eV, and all atoms in the slab were allowed to relax. The systems were considered to be fully optimized when the forces on each ion were smaller than 0.02 eV/Å.

The minimum energy pathways (MEP) were investigated using the climbing image nudged elastic band method (CI-NEB) to determine the transition state (TS) structure.[51,52] For both reactant and product of a certain reaction, we performed geometry optimization to identify the minimum energy configurations, which were then used to generate eight initial images along the MEP using linear interpolation. These atomic structures were relaxed subject to the CI-NEB constraints using the quasi-Newton scheme as the CI-NEB method requires a force-based optimizer.[51,52]

3. Results

This Cu ALD process consists of alternate pulses of precursor $Cu(dmap)_2$ and co-reagent Et_2Zn, separated by purges so that the two reagents are never simultaneously present in the gas-phase. Their mutual reaction thus takes places via adsorbates. Since $Cu(dmap)_2$ and Et_2Zn are introduced to the chamber in a sequential manner during the experiment, the full reaction cycle is divided into two sections. In section 3.1 we look at adsorption and decomposition (steps 1a and 1b) of $Cu(dmap)_2$ on bare Cu segments of the surface. In section 3.2 we investigate adsorption and decomposition of Et_2Zn (steps 2a and 2b), along with the series of surface reactions taking place between mixed fragments of $Cu(dmap)_2$ and Et_2Zn, followed by by-product formation and desorption (steps 1a and 2a). Step 1a thus regenerates a bare Cu(111) surface, ready for the repetition of step 1b. We therefore calculate the activation (E_a) and reaction energies (ΔE) of a series of surface reactions of the $Cu(dmap)_2$ and Et_2Zn on bare Cu(111) and identify reaction

pathways that have low enough activation energies to be viable at the experimental ALD temperature (393 K) in Ref [21]. Based on these calculations, we combine the reaction routes and propose the full ALD reaction cycle.

The steps in this cyclic process are labelled with capital letters from 'A' to 'G'. In the following sections, we separately present our results on each of these steps and discuss these reactions in order to understand the overall reaction mechanism of Cu ALD. Table 1 lists the calculated activation barrier (E_a) and the reaction energy (ΔE) for the selected reactions of $Cu(dmap)_2$ and Et_2Zn on the Cu(111) surface. Table 1S in Supporting Information displays the calculated activation barriers $E_a > 1$ eV (and associated reaction energies) that are too high for the surface reactions to occur in the ALD experiment.

Table 1. The calculated activation barriers (E_a) and reaction energies (ΔE) for possible reactions for depositing Cu from $Cu(dmap)_2$ and Et_2Zn through ALD. The data are plotted in Figure 2 and Figure 4. Capital letters 'A' to 'G' represent the following steps leading to atomic structures numbered A1, A2 etc: A is adsorption of $Cu(dmap)_2$ (Figure 3), B is decomposition of $Cu(dmap)_2$ (Figure 3), C is adsorption of Et_2Zn on the dmap–covered surface (Figure 5), D is the ethyl group migration (Figure 7), E is ligand diffusion (Figure 8), F is ligand re-ordering (Figure 9), G and H are $Zn(dmap)_2$ or butane formation (Figure 10 and Figure 10). The reactions with E_a less than 1.0 eV are shown here and in the figures; those with $E_a > 1$ eV are in Table 1S (supporting information).

reactions	**E_a (eV)**	**ΔE (eV)**	**explanation**
Section 3.1			
1. A1		-0.39	Physisorption of $Cu(dmap)_2$ from gas phase

2. A1→A2	0.17	-1.01	Physisorption to chemisorption transition
3. A2→B1	0.44	-0.11	One Cu–O bond scission Cu(dmap) + dmap
4. A2→B2	0.58	-0.01	Double Cu–O bond scission dmap +Cu +dmap
Section 3.2			
5. B1→C1		-0.03	Et_2Zn adsorption between Cu(dmap) + dmap
6. B2→C2		0.01	Et_2Zn adsorption between dmap+ Cu + dmap
7. C1→D1	0.78	-2.03	Butane formation and desorption
8. C1→D2	0.55	-0.65	ZnEt, CuEt, Cu(dmap), dmap formation
9. C2→D2	0.57	-0.69	ZnEt, CuEt, Cu(dmap), dmap formation
10. C1→D3	0.61	0.31	Two ethyl groups attached to the surface
11. D1→E1	0.34	-0.33	dmap ligand diffusion
12. D1→E2	0.68	0.28	dmap ligand diffusion
13. D2→E3	0.85	-0.68	Butane formation
14. D3→E4	0.33	0.20	dmap ligands diffusion
15. E1→F1	0.44	0.37	dmap ligands diffusion
16. E2→F2	0.62	0.28	dmap ligands diffusion
17. E3→F3	0.71	0.35	dmap ligands diffusion
18. E4→F4	0.56	0.30	$Zn(dmap)_2$ formation
19. F1→G1	0.78	0.43	dmap ligands re-ordering
20. F2→G1	0.15	0.05	dmap ligands re-ordering
21. F3→G1	0.32	-0.83	dmap ligands re-ordering
22. F4→G2	0.49	-0.38	Ethyl groups re-ordering
23. G1→H1	0.79	0.72	$Zn(dmap)_2$ desorption
24. G2→H2	0.73	-1.49	Butane desorption

Adsorption energies of Et_2Zn (reactions 5 and 6) on decomposed $Cu(dmap)_2$ is calculated relative to the configuration B1 with surface fragments of Cu(dmap) + dmap.

3.1. Adsorption and decomposition of $Cu(dmap)_2$ on Cu(111) surface

In the previous work, we studied the adsorption of $Cu(dmap)_2$ on a number of adsorption sites on flat and rough Cu surfaces using different levels of treatment of vdW interactions.[41] We found that pure PBE predicts that physisorbed and chemisorbed structures exist on the flat Cu(111) surface depending on the adsorption sites. We also found from the Bader charge analysis that the Cu atom in the molecule gains 0.2−0.4 electrons from the surface on chemisorption, which indicates that the adsorbate Cu atom is partially reduced when molecularly adsorbed. Now we discuss the possible reaction pathways of the adsorption of $Cu(dmap)_2$ onto segments of bare Cu(111) (configuration A) and its decomposition (configuration B) before reaction with Et_2Zn adsorbates. The energetics are illustrated in Figure 2.

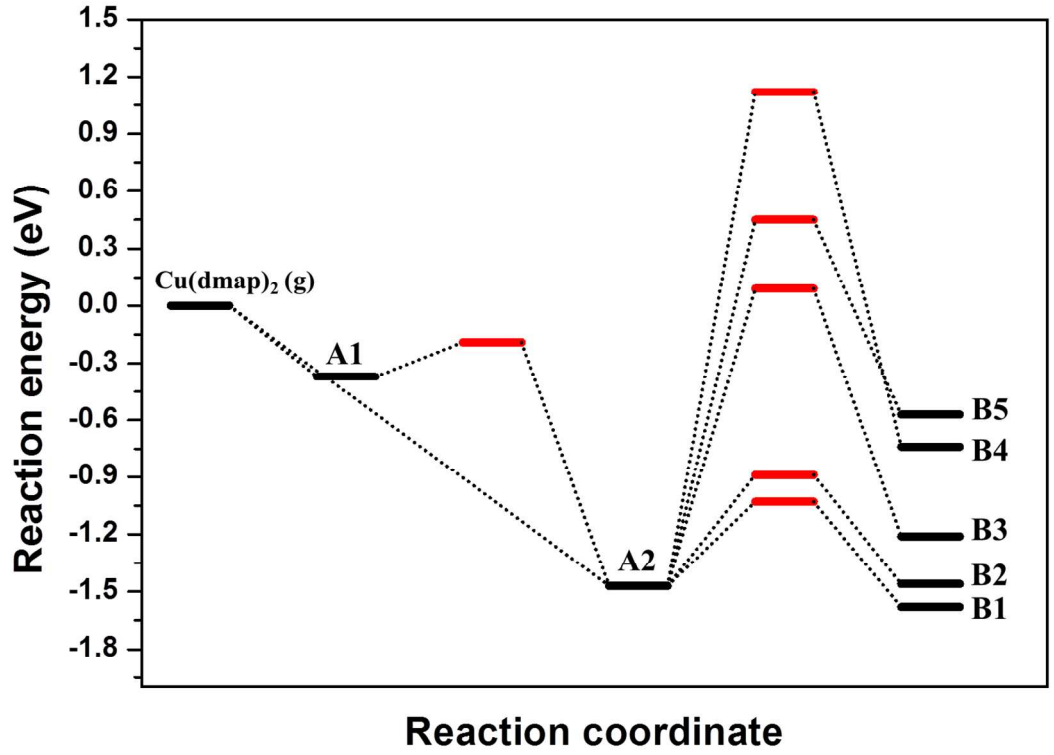

Figure 2. First half of the reaction cycle of Cu ALD for the $Cu(dmap)_2$ pulse. Reactant/product states are in black and activation energies are in red. Atomic structures for adsorption (A1, A2)

and decomposition (B1 and B2) are in Figure 3. The structures of B3, B4 and B5 are provided in Figure 1S.

A: Adsorption of $Cu(dmap)_2$. The physisorbed (A1) and chemisorbed (A2) structures are shown in Figure 3. The physisorbed $Cu(dmap)_2$ molecule is stable and not spontaneously reactive to Et_2Zn in our calculations. Therefore the physisorbed $Cu(dmap)_2$ molecules (A1) should transform into chemisorbed states (A2) if ALD is to take place. This involves the loosing of Cu – N coordination and the formation of metallic bonds from adsorbate Cu to surface Cu as described in detail in Ref [41]. Figure 2 shows that the transformation needs a small activation energy of 0.17 eV, which can be overcome at a typical ALD temperature, e.g. 100 °C.

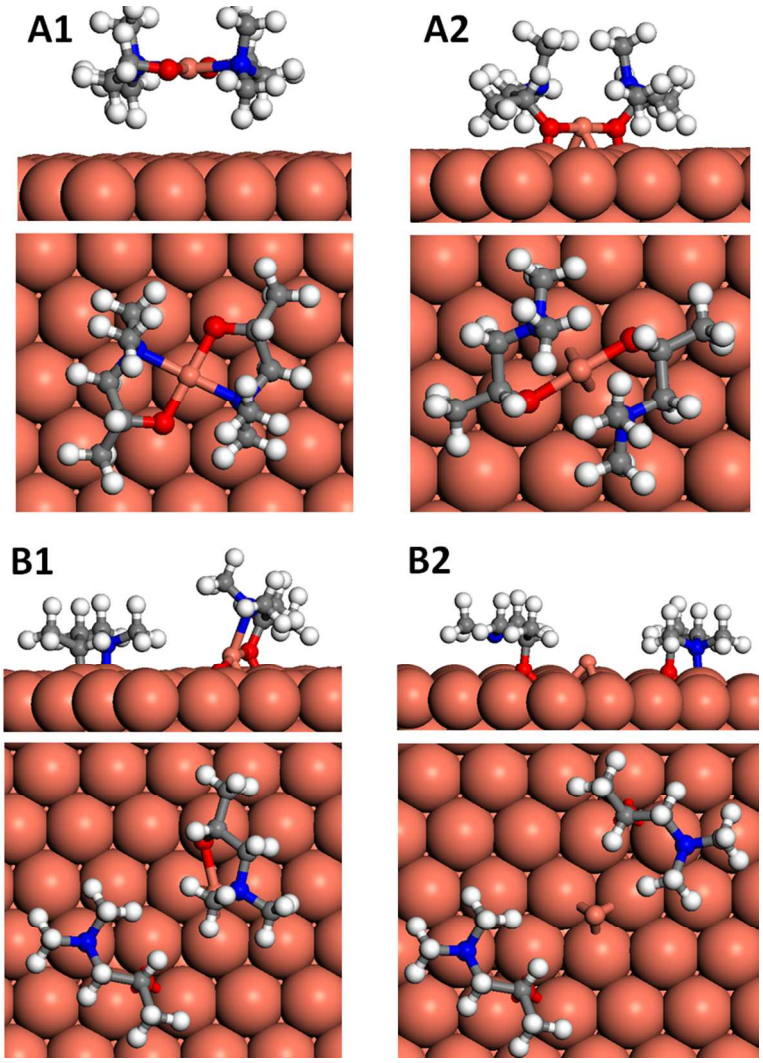

Figure 3. Adsorption (step A) and decomposition (step B) of $Cu(dmap)_2$ on one (6 × 6) cell of the Cu(111) surface. A1 represents physisorption and A2 represents chemisorption. The fragments of decomposed $Cu(dmap)_2$ are Cu(dmap) + dmap (B1) and dmap + Cu + dmap (B2). The colour code used throughout the paper and Supporting Information is as follows: salmon pink = copper, red = oxygen, blue = nitrogen, grey = carbon and white = hydrogen.

B: Decomposition of $Cu(dmap)_2$. The surface should be saturated with the chemisorbed $Cu(dmap)_2$ molecules or fragments after the $Cu(dmap)_2$ pulse in the ALD experiment. We found that Et_2Zn will not react with the chemisorbed $Cu(dmap)_2$ molecules on Cu(111). This is because

the Cu centre of the molecule is still not accessible, although the $Cu(dmap)_2$ molecule is partially decomposed upon chemisorption. Thus, it is legitimate to assume that the chemisorbed $Cu(dmap)_2$ undergoes further decomposition. We considered several possibilities for bond scissions in the $Cu(dmap)_2$ molecule: one Cu–O bond (B1), both Cu–O bonds (B2), O–C bond (B3), C–C bond (B4) and C–N bond (B5). We calculated the activation barriers for breaking one (A2→B1) and two (A2→B2) Cu–O bonds to be 0.44 eV and 0.58 eV, respectively, indicating that the reactions are both slow but viable at ALD temperatures. It was previously found that the dissociation of one acac ligand from $Cu(acac)_2$ on the Cu(110) surface requires an activation energy of 0.59 eV from PBE,[38] which is comparable to our finding for the dissociation of dmap ligand from $Cu(dmap)_2$ on Cu(111).

The optimized structures for the resulting configurations B1 and B2 are shown in Figure 3. In configuration B1, the surface is covered with the dmap and Cu(dmap) fragments of the molecule. The distance between the O atom in dmap and the Cu atom in Cu(dmap) is 4.45 Å, indicating that the Cu-O bond has broken. The O atom in the dmap is located in the hollow site of the Cu(111) surface and bonds with three surface Cu atoms. The Cu–N bond is re-formed (2.10 Å) again in the Cu(dmap) fragment because of a reduction of strain in the molecule upon the dissociation of the other dmap ligand.

In configuration B2, the distances of the O atoms in the dmap fragments from the adsorbate Cu atom are 3.95 Å and 3.99 Å, again indicating complete dissociation. Both the O atoms in the dmap fragments are bonding to Cu atoms of a hollow site. A bond between N and Cu surface atom is formed (2.31 Å) in one of the dmap ligands as is evident from Figure 3 where the Cu surface atom under the N atom is pulled up significantly. By comparing configurations B1 and B2 in Figure 3, we can see that the B1 configuration has a more dense coverage of dmap ligands

in the immediate locality of the Cu atom than the B2 configuration. Later we will show that this difference in the density of the ligands leads to two different reaction pathways. The reverse reaction to form the $Cu(dmap)_2$ molecule from these decomposed fragments is extremely unlikely because the forward reaction energies (ΔE) of A1→B1 and A1→B2 reactions are around -1.5 eV.

We now consider decomposition of a dmap ligand from chemisorbed $Cu(dmap)_2$ (A2). The calculated activation energies are 1.56 eV for the scission of the O–C bond (A2→B3), 1.92 eV for the scission of C–C bond (A2→B4) and 2.59 eV for the scission of C–N bond (A2→B5) (see Table S1 in Supporting information). The optimized structures of B3, B4 and B5 are displayed in Figure S1 in Supporting Information. Based on these E_a, the breaking of the O–C, C–C and C–N bonds are not accessible at a typical ALD reaction temperature of 100 °C, as in the work of Lee *et al*.[21] This indicates that the $Cu(dmap)_2$ molecules fragment instead through the breaking of one or two Cu–O bonds (B1 and B2) in ALD experiments. This shows that dmap ligands are 'innocent' and participate in the reaction as a single unit. Therefore in this work, decomposition of $Cu(dmap)_2$ refers to the dissociation of one or two Cu–O bonds in the $Cu(dmap)_2$ and not to break-up of dmap itself. At the end of the $Cu(dmap)_2$ pulse, we expect that the Cu(111) surface is saturated with the dmap and Cu(dmap) fragments of the precursor and that the further adsorption of $Cu(dmap)_2$ onto this surface is not possible due to Pauli repulsion. Therefore, as the Et_2Zn pulse starts, the Et_2Zn molecules may react simultaneously with the surface covered with partially and fully dissociated $Cu(dmap)_2$, namely Cu(dmap) + dmap (B1) and dmap + Cu + dmap (B2). B1 and B2 represent surfaces with different surface coverage of $Cu(dmap)_2$ precursors in the locality of Cu.

3.2. Et_2Zn adsorption, butane formation and $Zn(dmap)_2$ formation

Step 2a of the Cu ALD transmetalation process is proposed to be the reaction of Et_2Zn on the surface covered with fragments of $Cu(dmap)_2$ so as to deposit atomic Cu and formation of by-products butane and $Zn(dmap)_2$ (Equation 1). Step 1a consists of similar reactions of mixed ligands on a surface to reduce Cu and form by-products. We also investigate the formation of undesired by-products, which may result from parasitic reactions. Figure 4 shows the reaction energy pathways and values of activation and reaction energies are listed in Table 1, which we discuss in detail.

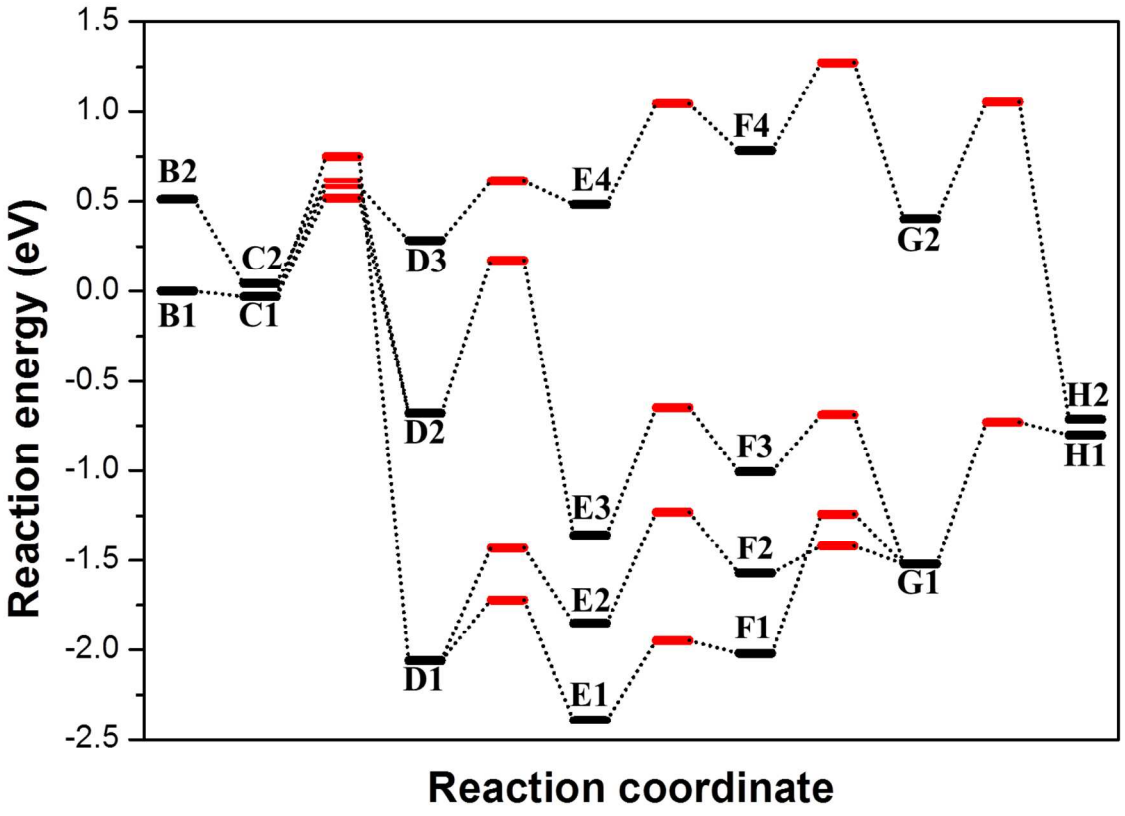

Figure 4. Reaction energy diagram for the second half reaction cycle of the Cu ALD process when Et_2Zn is admitted. Reactant/product states are in black and activation energies are in red. Forward activation energies greater than 1 eV are not included in the graph. The configurations labelled with a capital letter and number are shown in the following figures.

C: Adsorption of Et_2Zn on the dmap–covered surface (step 2a). Figure 5 shows the optimized structures of Et_2Zn adsorption on the configurations B1 and B2, which are labelled C1 and C2, respectively. The adsorption energies are calculated to be -0.03 eV and +0.01 eV, respectively. These small adsorption energies are apparently the result of distortions of both dmap ligands and of the Et_2Zn molecule on the surface. In the C1 configuration, the Et_2Zn molecule is adsorbed between the Cu(dmap) and dmap fragments. The Zn atom in the Et_2Zn molecule is situated on a bridge site of Cu(111). The ethyl groups are bent upward and the ∠C-Zn-C angle is 134.5°. The distance between Zn and the adsorbate Cu atom is 3.11 Å. The Zn – O distances are 4.01 Å and 4.35 Å. Notice that the ethyl groups in configuration C1 have no chemical bond with the surface. In configuration C2, the Et_2Zn molecule is attached on top of the adsorbate Cu atom. The adsorbate Cu atom forms bonds with the Zn atom (Zn–Cu bond length is 2.43 Å) and with the C atom (C –Cu bond length is 2.12 Å) in one of the ethyl groups to form a 3-membered ring. This results in substantial stabilization relative to B2. The difference in the adsorption geometry between C1 and C2 results from the lower local coverage of the dmap ligands on the C2 surface. As will be shown in the next section, this has a substantial effect on subsequent reaction kinetics. However, overall, the C1 and C2 structures are very close in energy.

In the C1 and C2 structures, Et_2Zn is found to adsorb on Cu atoms close to $Cu(dmap)_2$ fragments. This is because we assume that before step 2a the surface is saturated with the $Cu(dmap)_2$ precursor after the first pulse. (See reaction E→F below for the kinetics of dmap diffusion). However, during an ALD experiment dmap should desorb as $Zn(dmap)_2$ and the coverage of dmap will drop, and therefore the Et_2Zn molecules of step 2b may adsorb on a bare segment of the surface. Thus, we also investigate the adsorption of Et_2Zn on the fully bare

Cu(111) surface. The Et_2Zn molecules decompose into Et and ZnEt fragments spontaneously upon adsorption onto Cu(111) without the presence of $Cu(dmap)_2$ fragments (see the adsorption structure in Figure S2, Supporting information) and the adsorption energy is -0.83 eV. This mode of decomposition of Et_2Zn into Et and ZnEt fragments structure was also found in previous *ab initio* molecular dynamics study on a model of bare Cu(111).[36]

This indicates that the presence of $Cu(dmap)_2$ fragments (B1 and B2) prevents the full decomposition of Et_2Zn and permits that the Et groups to stay attached to the Zn atom, as shown in the C1 and C2 structures. The $Cu(dmap)_2$ fragments are affected by the adsorption of the Et_2Zn molecule as the CH_3 parts of the dmap ligands shift slightly upward.

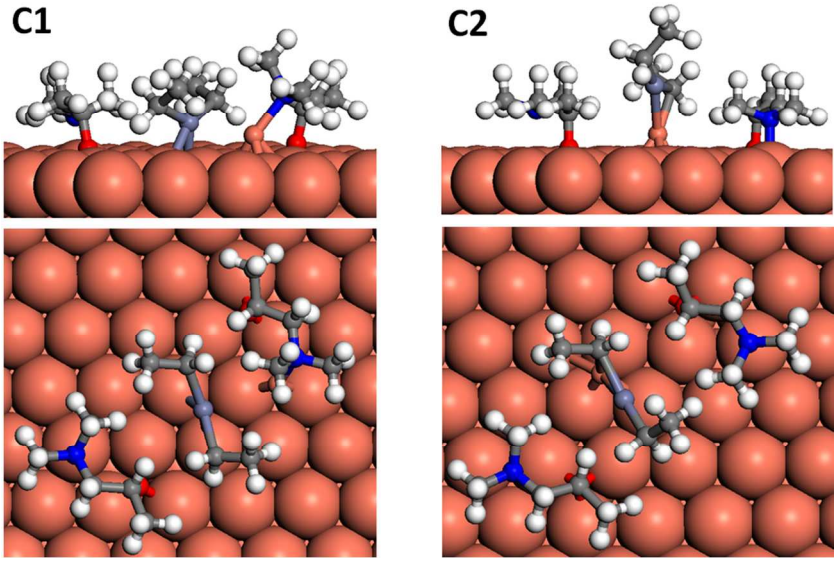

Figure 5. Step C: Adsorption of Et_2Zn on the surface with fragments of $Cu(dmap)_2$ from B1 and B2, respectively.

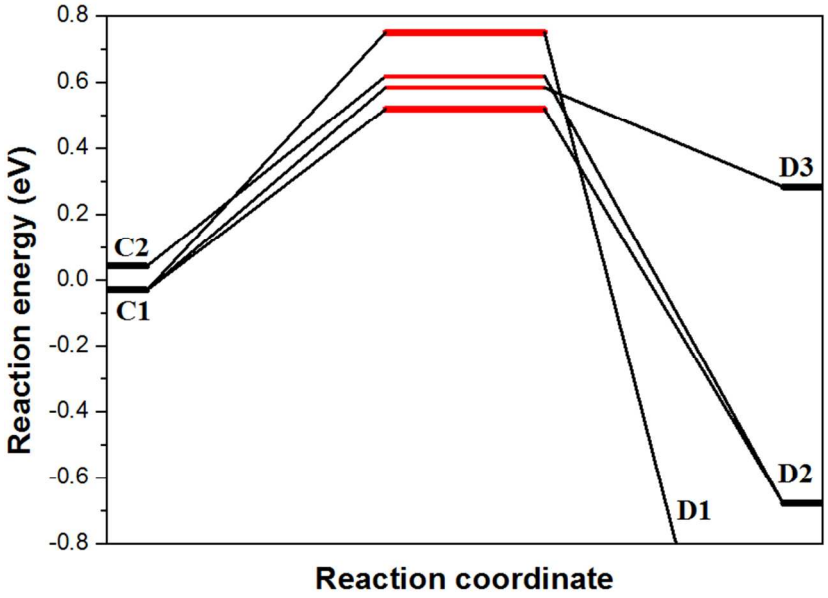

Figure 6. Reaction energy diagram from step 'C' to step 'D'. This is the magnification of the process from 'C' to 'D' in Figure 4.

D: The ethyl group migration (step 1a & 2a). As the Zn atom is attached to ethyl groups in configurations C1 and C2, the ethyl groups must migrate away from the Zn atom in order to give the dmap ligand access to Zn and allow the ethyl groups to form butane, one of the by-products of Equation (1). We consider several possibilities for ethyl group migration: (1) direct butane formation from Zn and desorption (C1→D1); (2) one ethyl migration to adsorbate Cu to form CuEt and ZnEt fragments (C1→D2 and C2→D2) and (3) migration of both ethyl groups to surface Cu (C1→D3). The reaction energy diagram for this part is magnified from Figure 4 and shown in Figure 6 and the final configurations D1, D2 and D3 of ethyl group migrations are shown in Figure 7.

The direct formation of butane (C1→D1) is highly exothermic (ΔE = -2.03 eV, Table 1), and needs activation energy of 0.78 eV. (The reaction energy profile of this step is plotted in Figure S2 in Supporting Information). Electrons are transferred from desorbing ethyl groups to the

surface Zn atom. The distance between butane molecule and the surface in the D1 structure is 5.6 Å, indicating that the butane molecule has no interaction with the surface and can be purged away during ALD experiment. The deposited Zn atom forms a bond with the Cu adatom with the bond length of 2.6 Å. This direct formation of butane is a less likely scenario from configuration C2, as evidenced by the calculated activation barrier of 1.25 eV (C2→D1, Table S1, Supporting Information). This is because an extra C – Cu bond was formed when the Et_2Zn adsorbed on the Cu adatom in configuration C2. This is an important result because it shows the effect of surface coverage (C2 vs C1) on the kinetics of formation of butane. As noted in the previous results, at very low coverage, *i.e.* on segments of bare Cu, Et_2Zn dissociates spontaneously into ZnEt + CuEt, resulting in an even higher barrier to Et formation.

In the second case, formation of CuEt and ZnEt fragments attached to the surface (configuration D2) was achieved from both C1 and C2, with activation energies of 0.55 eV and 0.57 eV, and reaction energies of ΔE = -0.7 eV. In the C1→D2 reaction, one Et group from the adsorbed Et_2Zn migrates to the Cu adatom in Cu(dmap), which in turn causes the Cu-N bond to break, displacing the dmap ligand to bind with surface Cu. The D2 surface is thus covered with four fragments: two dmap ligands, ZnEt and CuEt groups. The ZnEt part of Et_2Zn molecule migrates to the surface by scission of C-Zn and Cu-Zn bonds.

The configuration D3, where the two ethyl groups have migrated to the Cu(111) surface, was reached from configuration C1 with an activation energy of 0.61 eV and reaction energy of +0.31 eV. Thermodynamics thus favours the reverse reaction from D3 to C1, or indeed to D2. We found that achieving D3 from C2 is kinetically impossible, requiring an activation energy of 1.78 eV (Table S1 of Supporting Information), probably because this would re-expose the adsorbate Cu atom.

Now we consider butane formation when no $Cu(dmap)_2$ fragments are around the adsorbed Et_2Zn so as to quantify the role of $Cu(dmap)_2$ fragments on the energetics of butane formation. Figure S2(b) displays the reaction energy profile of butane formation on the bare Cu(111) surface. Without the dmap ligands, butane formation needs higher activation energy and is less exothermic (E_a = 0.99 eV and ΔE =-1.14 eV) compared to the butane formation (C1→D1) from the Et_2Zn adsorbed in the neighbourhood of $Cu(dmap)_2$ fragments (see also Table S1, Supporting Information). We can explain this by noting that the adsorbed Et_2Zn decomposes into Et and ZnEt fragments when adsorbed on the bare surface, so that the formation of butane apparently becomes more difficult because breaking the C – Cu surface bond needs extra energy. The distance between the butane molecule and the surface with the presence of $Cu(dmap)_2$ fragments is longer by 1.4 Å compared to that on the bare Cu(111) surface. Thus, butane formation requires lower E_a when the $Cu(dmap)_2$ fragments are nearby. This indicates that the dmap ligands play a cooperative role[53] for the formation of butane.

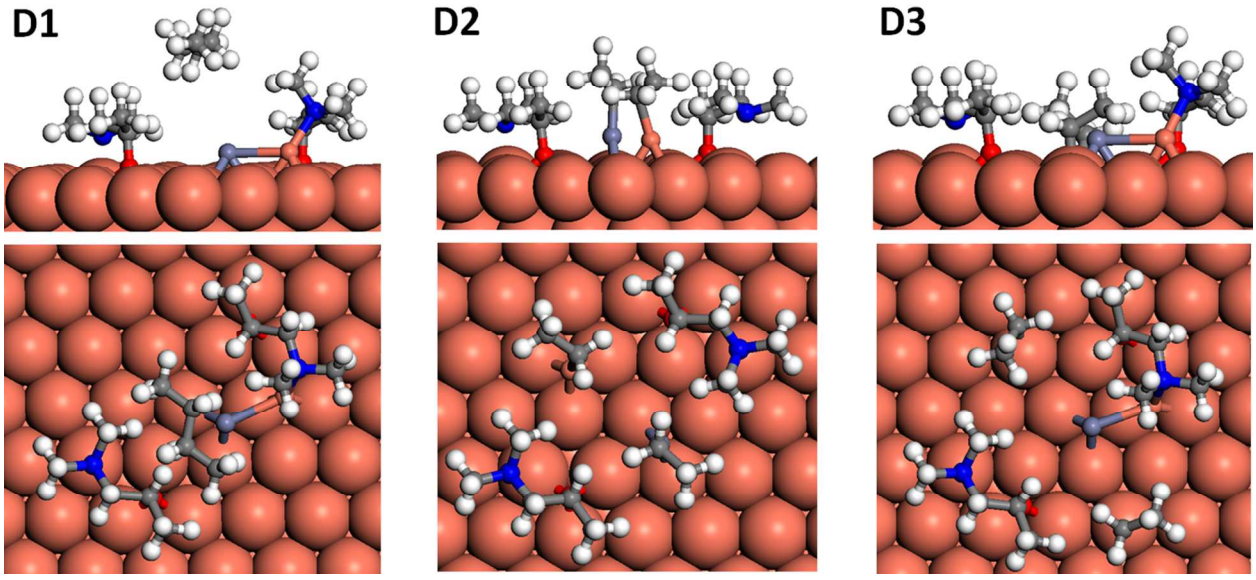

Figure 7. Step D: reaction of Et_2Zn obtained from configuration C1 and C2. Three possibilities are considered: D1 is butane formation; D2 is ZnEt + CuEt fragment formation and D3 has fragments of two ethyl groups on the Cu(111) surface.

A visual inspection of configurations D2 and D3 (Figure 7) shows that there is space in the (6 × 6) simulation cell for two adsorbed ethyl groups and two dmap ligands. It should therefore be possible to accommodate at least four ethyl groups in such a cell when dmap has been eliminated, even if diffusion of Et groups is slow. We use this result later to estimate the ALD growth rate.

E: ligand diffusion. Once the Zn atom becomes accessible for dmap ligands, dmap ligands may diffuse on the surface to form a $Zn(dmap)_2$ molecule, which is the other by-product in equation (1). Figure 8 shows the configurations of relevant reaction products obtained from D1, D2 and D3 configurations. The configurations E1 and E2 are obtained from D1 by moving dmap ligands after removing the butane molecule. In configuration E1, a dmap ligand moves toward the Zn atom (D1→E1), which involves an activation energy of 0.34 eV and reaction energy of ΔE = -0.33 eV. This low barrier shows that dmap ligands can diffuse on the bare Cu(111) surface

to render the $Zn(dmap)_2$ by-product under mild ALD conditions. The activation energy for D1→E2 is twice greater than that of D1→E1. This is because the dmap ligand in the D1→E2 process has to move above the Cu-Zn dimer instead of along the smooth Cu(111) surface, which makes the diffusion of dmap more difficult. In the E2 structure, the O atom in Cu(dmap) attaches to the Zn atom and a trimer of Zn-Cu-O is formed.

We investigated whether the two ethyl groups attached to the Cu and Zn in the D2 structure can combine to yield a butane molecule (E3). The reaction is exothermic (ΔE = -0.68 eV), but not as much as other steps that yield butane (ΔE = -2.03 eV for C1→ D1 and ΔE = -1.49 eV for G2 → H2) and the computed activation energy is high (E_a = 0.85 eV). This suggests that ZnEt resists loss of the Et ligands. The Cu to Zn distance is 4.47 Å and the distances between O atoms in the dmap ligand and the Zn atom are 4.22 Å and 4.69 Å in configuration E3.

Because the D2 configuration has a complex surface structure consisting of two dmap, CuEt and ZnEt fragments, we check the viability of parasitic reactions to form (dmap)CuEt and (dmap)Et intermediates. Although the formation of the (dmap)CuEt intermediate adsorbate is found to be possible with the E_a = 0.44 eV and ΔE = +0.16 eV, the desorption of that molecule is unlikely as it needs an activation energy E_a of 2.25 eV (Table S1, Supporting information). Since formation of this (dmap)CuEt adsorbate is endothermic (ΔE = +0.16 eV), it is likely that the reverse reaction from this intermediate product to CuEt, Cu(dmap) and ZnEt in configuration D2 may take place with the reverse activation barrier E_a = 0.28 eV. This means that (dmap)CuEt is transient and decomposes, returning to the D2 configuration. We also found that the formation and desorption of (dmap)Et is not accessible because it also faces a high barrier (E_a = 1.82 eV, Table S1 Supporting Information). This supports the assumption in Figure 1b about the by-

products of ALD. Therefore, butane formation (D2→E3) is the most likely step from the D2 configuration, albeit kinetically hindered.

For configuration E4, two dmap ligands from D3 diffuse toward the Zn atom to form the $Zn(dmap)_2$ molecule, with an activation energy of 0.33 eV and ΔE = +0.20 eV. Through the endothermic reaction pathway B1→C1→D3→E4, the $Zn(dmap)_2$ may be formed as the ethyl groups are donated to the copper surface.

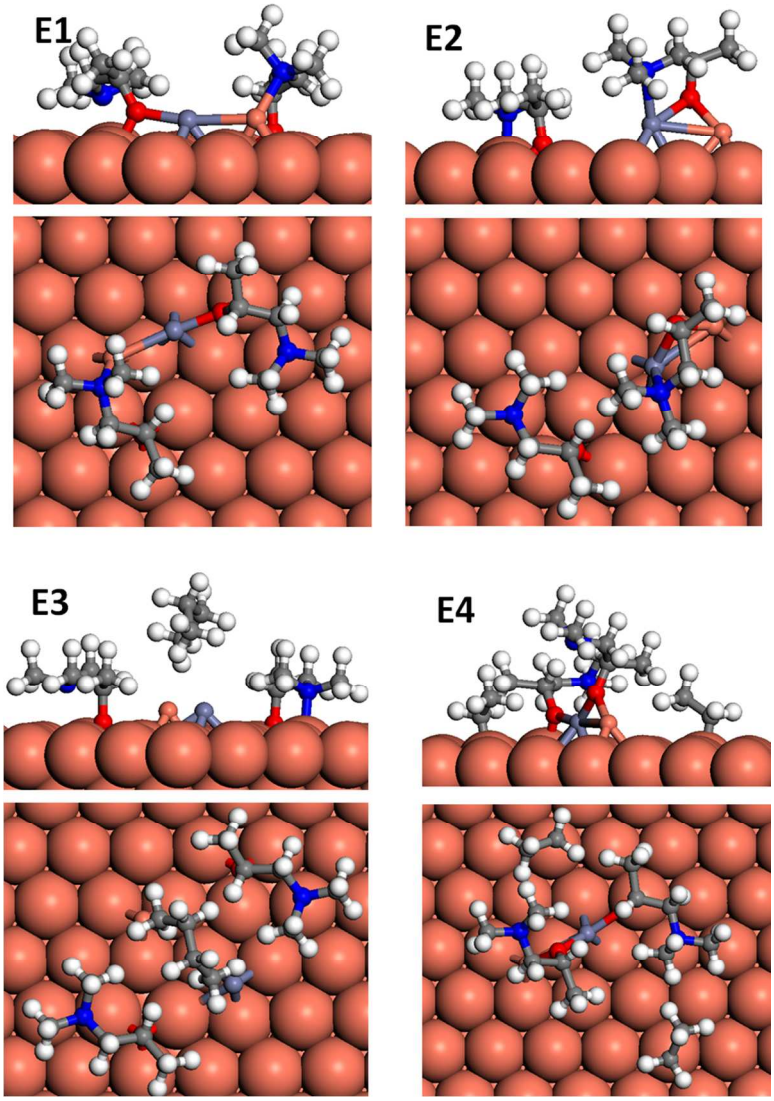

Figure 8. step E: ligand diffusion. E1 and E2 are reaction products of D1. E3 and E4 are the reaction products of D2 and D3, respectively.

F: Ligand re-ordering (step 1a & 2a). Although dmap ligands have diffused toward the Zn atom in the previous step, the $Zn(dmap)_2$ molecule is not yet formed because the Zn atom is not coordinated with both the O and N atoms in the dmap ligands. Therefore after the dmap ligands have diffused towards the Zn atom, they may re-order their atomic positions to form a $Zn(dmap)_2$ molecule. Figure 9 shows the re-ordered dmap ligands around the Zn atom.

The E1 $\rightarrow$ F1 reaction consists of the migration of dmap from adatom Cu to the Zn atom and needs activation of 0.44 eV. The reaction is endothermic with ΔE = 0.37 eV. As we can see from the F1 configuration, the $Zn(dmap)_2$ structure is still deformed and the N–Zn distances are 1.9 Å and 3.8 Å, respectively.

The reaction E2 $\rightarrow$ F2 involves the scission of the Zn-Cu bond and re-ordering of dmap ligands so that the O atom in dmap forms a bond with the Zn atom, which needs E_a of 0.62 eV. In this case, the long O–Zn distance is 4.2 Å. Thus, to form the F2 configuration, the ligands have to move further than E1 $\rightarrow$ F1 to form the $Zn(dmap)_2$ molecule.

The F3 configuration is obtained after removing the butane molecule in the E3 structure and optimizing the geometry. The O atoms in the dmap ligands are attached to the Zn atom in the F3 configuration. The process E3 $\rightarrow$ F3 is slightly endothermic with a reaction energy of +0.35 eV, and an activation barrier of 0.71 eV.

In the F4 configuration, the $Zn(dmap)_2$ by-product molecule is formed in the presence of two ethyl groups on the surface. Obtaining F4 from E4 needs an E_a of 0.56 eV and ΔE of +0.30 eV. Comparing F4 with the F1, F2 and F3 structures, we can see that the F4 adsorbate is the closest in structure to $Zn(dmap)_2$, as is evident from the formation of all Zn – O (1.97 Å) and Zn – N (2.29 Å) bonds. We note that the surface in F4 is more crowded with the presence of Et groups and this may facilitate the formation of $Zn(dmap)_2$.

Overall, during the E → F process, the dmap ligands re-order around Zn to form the $Zn(dmap)_2$ molecule prior to desorption (step G). However, this process is endothermic with reaction energies of +0.3 to +0.4 eV and needs high activation energies ranging between 0.4 and 0.8 eV. This suggests that diffusion of dmap across the surface is slow and that perfect packing of dmap ligands may not be achieved over the timescale of the $Cu(dmap)_2$ pulse. Small sections of bare Cu may therefore still exist on the surface at the end of step 1b.

The energetics of E → F also indicate that the overall formation of $Zn(dmap)_2$ is a relatively slow process. The reverse reactions F → E will therefore happen with the higher reaction rate than E → F. This may result in residual dmap ligands blocking surface sites at the end of the Et_2Zn pulse, which in turn will block further adsorption and reduce the overall ALD growth rate. At low temperature therefore, some of the dmap ligands may not be desorbed and may remain inside the deposited Cu thin film in some form. This may also explain C and O incorporation into Cu thin films which is observed in experiment below temperatures of 100 °C.[20] However, our calculations do not explain why C and O impurities are also detected experimentally at temperatures above 130 °C. In addition, residual Zn cations may be reduced to Zn metal and incorporated as an impurity. This too was observed in growth experiments (8 – 15 % Zn impurity at 120 – 150 °C).[20]

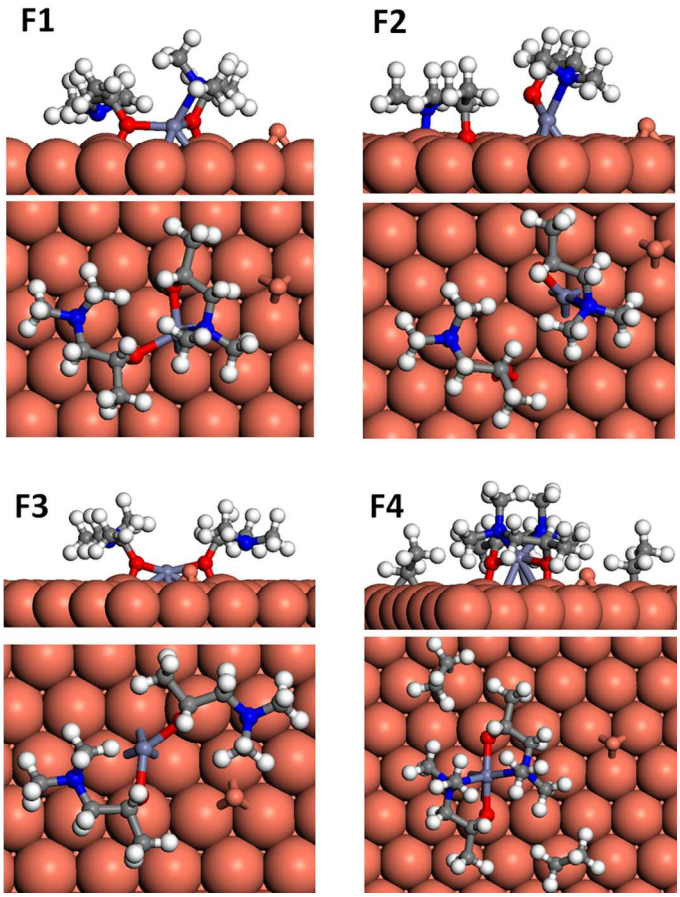

Figure 9. Step F: ligand re-ordering. Configuration F1 and F2 are reaction products of E1 and E2, respectively. F3 configuration is obtained after removing the butane molecule in E3. F4 is obtained from E3.

G: $Zn(dmap)_2$ or $Cu(Et)_2$ formation at the surface (step 1a & 2a). After ligand diffusion and ligand re-ordering steps, a $Zn(dmap)_2$ molecule can be formed from these re-ordered ligands. In the F1, F2 and F3 configurations, the O atoms of dmap ligands attach to the Zn atom and only the spatial arrangements of dmap and Zn(dmap) fragments differ slightly. Thus these three structures can re-order so as to yield a single configuration G1, as shown in Figure 10. The activation energy for achieving G1 from F1 (0.78 eV) is approximately twice greater than that of achieving G1 from F3 (0.32 eV). The process F2 → G1 only needs an activation energy of 0.15

eV because the Zn atom is already coordinated to the ligand in the F2 configuration. The two processes of $Zn(dmap)_2$ formation from F1 and F2 are endothermic with reaction energies of +0.43 eV and +0.05 eV, respectively. In configuration G1, $Zn(dmap)_2$ is not fully shaped, as one of the Cu–N distances is greater than its gas phase bond length by 1.6 Å. By comparing the $Cu(dmap)_2$ chemisorbed on Cu(111) with configuration G1, we can find that it has some common features: O–Zn–O atoms form bonds with the surface Cu atoms, and N–containing parts of the ligand are distorted. This indicates that G1 is indeed the chemisorbed $Zn(dmap)_2$ on the Cu(111) surface. Next in the proposed mechanism, this chemisorbed $Zn(dmap)_2$ molecule should desorb from the surface (step H).

The ethyl groups or the deposited Cu adatom migrate to form a an adsorbed $Cu(Et)_2$ unit in configuration G2, which follows the desorption of the $Zn(dmap)_2$ molecule in configuration F4. We found that formation of butane from ethyl groups on the smooth surface is not kinetically favourable, because it needs an activation energy of 0.99 eV (Table S1 in Supporting Information). However in G2, the deposited Cu adatom can diffuse on the surface with a relatively small energy cost (E_a = 0.02 eV from one hollow site to the neighbouring hollow site), and so we moved the deposited Cu adatom between the two ethyl groups to form the $Cu(Et)_2$ intermediate. The activation barrier to form the $Cu(Et)_2$ adsorbate in configuration G2 from F4 (after removing the $Zn(dmap)_2$ molecule and moving the deposited Cu adatom between two ethyl groups) is 0.49 eV. The reaction is moderately exothermic with reaction energy of -0.38 eV. Comparison with the barrier for smooth surfaces (E_a = 0.99 eV) indicates that butane formation is only possible on rough surfaces during the ALD process.

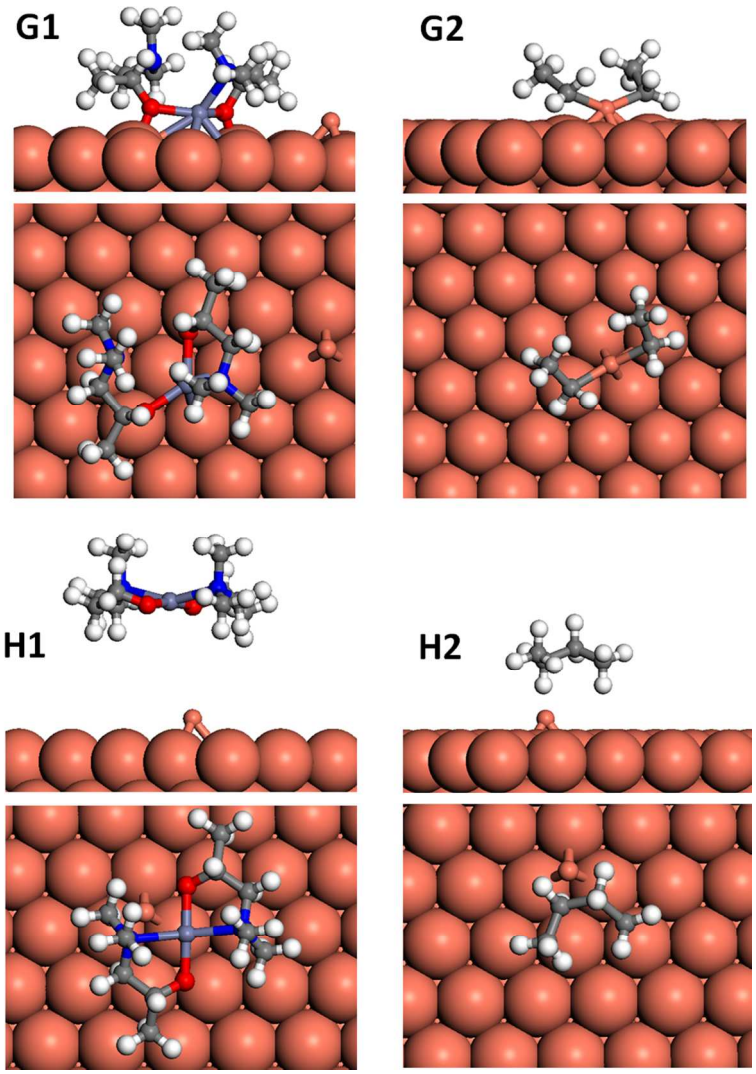

Figure 10. By-product formation (step G) and desorption (step H). G1 which is obtained from F1, F2 and F3 configurations shows the formation of $Zn(dmap)_2$. G2 is obtained after the formation and desorption of the $Zn(dmap)_2$ molecule in F4 configuration. As the diffusion of Et groups on bare Cu(111) is not preferred, the $Cu(Et)_2$ intermediate product is formed by diffusion of the Cu adatom or Et group. H1 and H2 structures are obtained from G1 and G2, respectively.

H: $Zn(dmap)_2$ or butane desorption (step 1a & 2a). In the G1 configuration above, dmap ligands re-ordered to form chemisorbed $Zn(dmap)_2$ and in H1 this molecule desorbs (Figure 10). It is found that the desorption of $Zn(dmap)_2$ from the smooth surface needs an activation energy

of 1.34 eV, which makes it not possible under the experimental condition. As the diffusion of deposited Cu adatom on the Cu(111) surface is nearly barrierless, we moved the Cu near the Zn atom in G1. The reaction energy ΔE of $Zn(dmap)_2$ desorption with the help of the Cu adatom is +0.72 eV and the computed barrier E_a (0.79 eV) is almost the same, (*i.e.* the adsorption of $Zn(dmap)_2$ would be barrierless). The Zn–O and Zn–N bond distances are 1.89 Å and 2.30 Å, respectively. The desorbed $Zn(dmap)_2$ by-product molecule can be purged away to vacate the surface for new precursor molecules (Et_2Zn in step 2b, $Cu(dmap)_2$ in step 1b).

In the H2 configuration, which is obtained from configuration G2, the butane molecule desorbs through the decomposition of the $Cu(Et)_2$ molecule into butane, which needs quite a high activation energy of 0.73 eV. The G2 → H2 process is strongly exothermic with ΔE = -1.49 eV, consistent with the other process of butane desorption C1 → D1. Reduction of the surface as a whole takes place when two ethyl anions combine and desorb as neutral butane. Once again, reduction of the surface cations to metallic Cu is achieved in this step by donation of electrons from ethyl groups as they combine into butane and desorb.

4. Discussion

The reaction mechanism of Cu ALD

The results for step 1b (Section 3.1) show that the $Cu(dmap)_2$ pulse seems to involve dissociative chemisorption of the complex into Cu(dmap) and dmap (B1 and B2), leaving the ligands intact. Dissociation within the dmap ligand is thermodynamically not preferred (Figure 2), implying that the transmetalation reaction may take place as proposed in Eq. 1. In the original experimental work,[21] the film thickness increment per cycle for $Cu(dmap)_2$ is saturated when the pulse time exceeds 2 s which allows the full saturation of the surface with the fragments of

$Cu(dmap)_2$. These thermodynamically stable fragments prevent the further adsorption of precursor.

During step 2a of the second pulse, the Et_2Zn reducing agent reacts with the Cu(dmap) and dmap fragments and a range of reactions may take place, as shown in Figure 4 and presented in section 3.2. In the experimental work,[21] the pulse time for Et_2Zn is 0.5 s and Et_2Zn undergoes self-terminating replacement reaction with the $Cu(dmap)_2$ adsorbed on the surface. An early formation of the butane molecule (D1) is predicted to be possible just after adsorption of Et_2Zn; this reaction is extremely exothermic but faces a high kinetic barrier and deposits a Zn atom near dmap and Cu(dmap) fragments. Alternatively, the butane molecule may be formed during the D2 $\rightarrow$ E3 step after the Et_2Zn dissociates into ZnEt and Et fragments at the surface.

We also found that parasitic reactions including the formation of (dmap)Cu(Et) and (dmap)(Et) face such high activation barriers that they are not feasible under ALD conditions.

After butane formation and desorption, the dmap ligands diffuse toward the Zn atom and form Zn – O and Zn – N bonds to yield the $Zn(dmap)_2$ molecule, which finally desorbs from the Cu surface. These reactions (D1 $\rightarrow$ E1 $\rightarrow$ F1$\rightarrow$ G1, D1 $\rightarrow$ E2 $\rightarrow$ F2 $\rightarrow$ G1 and D2 $\rightarrow$ E3 $\rightarrow$ F3 $\rightarrow$ G1) have activation barriers ranging from 0.3 eV to 0.8 eV, and they are mostly endothermic. This reaction pathway is schematically illustrated in Figure 11a.

For the reaction route involving the D3 structure which has two ethyl groups, dmap and Cu(dmap) fragments attached to the surface relatively spaciously, we introduce a different reaction mechanism based on reaction routes between D3 and H2, which is displayed in Figure 11b. During the C1$\rightarrow$ D3 step, the ethyl groups migrate away from Zn to the surface. This provides dmap ligands with access to diffuse toward the under-coordinated Zn atom and re-order

to form the $Zn(dmap)_2$ molecule during the next steps (D3→ E4 and E4→ F4). Desorption of $Zn(dmap)_2$ produces a rather bare Cu surface with a low coverage of Et groups.

It is found that the formation of butane on the smooth Cu surface is not kinetically accessible, in contrast to the cooperative role of dmap ligands in step C1→ D1. The formation of the intermediate product $Cu(Et)_2$ with the help of a migrating Cu atom reduces the activation energy needed for the formation of butane because this causes the interaction between the Et groups and the surface to weaken. The butane desorption in the F4→ G2 reaction is again extremely exothermic, consistent with the step C1→ D1.

The reaction mechanisms shown in Figure 11a and Figure 11b are two possible routes for the copper ALD reaction proposed in Equation (1). These two different reaction mechanisms stem from the different coverage of dmap ligands, as we can see from the B1 and B2 configurations in Figure 3. The reaction mechanism in Figure 11a originates from the surface with relatively dense ligands and the reaction mechanism in Figure 11b results from the surface less densely saturated ligands. As we will discuss later, these two types of reaction mechanisms are direct results of cooperative effects determined by the different coverage of ligands on the surface.

As we can see from Figure 4, the reaction energies of most of the ligand diffusion and ligand re-ordering steps leading to $Zn(dmap)_2$ (D→ G) are positive and the reaction pathways are uphill in these stages. This means that the activation barriers for the reverse reactions are smaller than those of the forward reactions and so the reaction rates of the reverse reactions can be higher than those of the forward reactions during the ligand diffusion and re-ordering steps. Nevertheless, desorption of $Zn(dmap)_2$ is expected to be irreversible, and this will drive the equilibrium towards formation of the product (H1). Even so, residual adsorbed dmap (D1) may block sites against adsorption of $Cu(dmap)_2$ in the next ALD cycle. There is recent theoretical[53]

and experimental[54] evidence that ligands persist for multiple cycles in some ALD processes. Slow re-ordering and desorption of the Zn by-product may result in incorporation of Zn into the growing metallic film as an impurity. Indeed 8 - 15 % Zn is detected in the experiment.[20]

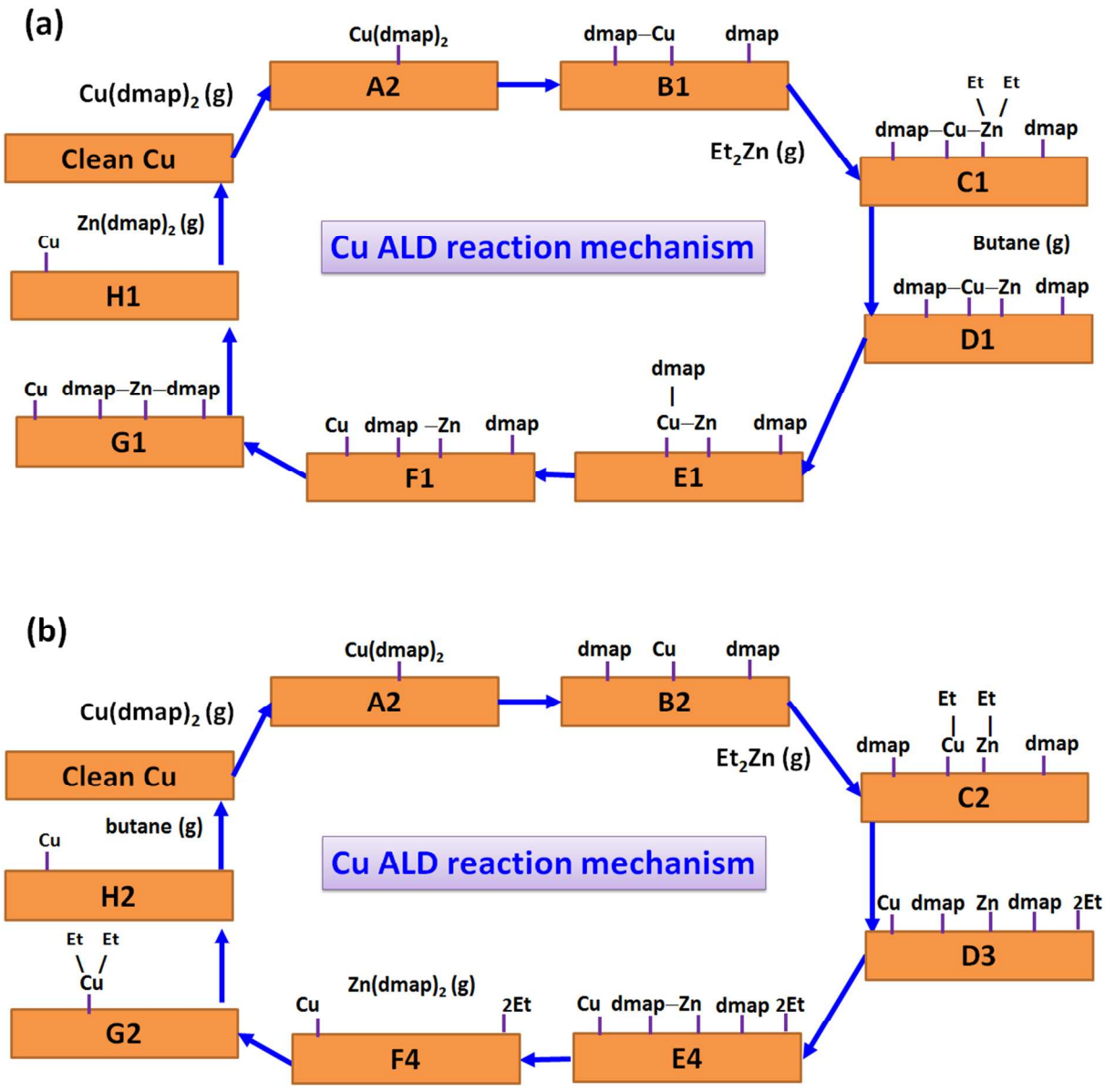

Figure 11. The reaction mechanisms of copper ALD from $Cu(dmap)_2$ and Et_2Zn. The capital letters and numbers inside the boxes represent the structures shown in Figure 3 to Figure 10. The mechanism in (a) corresponds to reactions with densely adsorbed precursors in the immediate

locality of the Cu atom and the mechanism in (b) corresponds to the reactions of the less densely adsorbed precursors.

Estimate of ALD growth rate

Having obtained evidence for the ALD cycle of Figure 1b and likely coverages of ligands at the end of each step of the cycle, we are now able to estimate the growth rate of Cu in each cycle. Each Cu^0 atom deposited in step 1a is the result of the reductive elimination of two Et groups as butane. The reaction is therefore limited by the coverage of Et groups at the end of step 2b, which we conservatively estimate at four Et groups per (6 × 6) simulation cell (section 3.2), meaning 2 Cu atoms deposited per cell. Further adsorption of $Cu(dmap)_2$ is possible in step 1b (for reduction to Cu^0 in step 2a), although we suggest that this is limited by the availability of sufficiently large segments of bare Cu. Adsorption of one $Cu(dmap)_2$ molecule per (6 × 6) cell blocks further adsorption, which gives a reasonable estimate for the amount of Cu deposited in step 1b. The total amount deposited per cycle is therefore three Cu atoms per (6 × 6) cell, or 3/36 of a monolayer. Since the height of one monolayer of crystalline Cu in the (111) direction is 2.10 Å in experiment, the predicted growth rate is 3/36 of this, *i.e.* 0.18 Å/cycle. This agrees remarkably well with the experimental growth rate of 0.2 Å/cycle,[21] which may be fortuitous, given the many assumptions feeding into the predicted value. Nevertheless, this result illustrates that the proposed ALD cycle can account for the experimental growth rate.

The impact of vdW interaction

In this work, we used pure PBE to calculate the activation barriers and reaction energies for $Cu(dmap)_2$ and Et_2Zn interacting with a Cu surface. In our previous work, we found that the vdW interaction is an important factor in describing the adsorption of $Cu(dmap)_2$ on copper surfaces.[41] Therefore, we now test the impact of vdW interaction on the energetics of the

dissociation of one dmap ligand from the $Cu(dmap)_2$ molecule adsorbed on Cu(111) (A2→B1) by using the optB88-vdW method. For this reaction, the optB88-vdW method yields an activation energy E_a = 0.55 eV, which is slightly larger than the PBE value of 0.44 eV, and a reaction energy of ΔE = -0.10 eV, which is approximately the same as the PBE calculated ΔE of -0.11 eV. Hu *et al.* used PBE and vdW-DF to calculate the activation barriers for the dissociation of $Cu(acac)_2$ on the Cu(110) surface and found that vdW-DF gives a slightly lower activation barrier than PBE.[38] However, they found that PBE and vdW-DF produce energy profiles with similar trends for the dissociation of the $Cu(acac)_2$ molecule. Slightly different activation energies but the same trend in energy profiles were also found with vdW-inclusive DFT methods in other computational works.[55,56] Thus, we argue that inclusion of vdW interaction in DFT may have a small effect on the values of the activation energies, but that the nature of the reaction mechanisms described in Figure 11 will probably not be affected.

Cooperative role of ligands

It was previously reported that the cooperation between adsorbates plays an important role in the kinetics of ALD reactions for oxides.[53] Inert adsorbed fragments become reactive once sufficient numbers of precursors adsorb in their neighborhood. It was not previously known whether ligand-covered metal surfaces show the same magnitude of cooperative effect as ligand-covered oxide surfaces. Although we studied the reaction of just one $Cu(dmap)_2$ and one Et_2Zn molecule on a 2 nm^2 section of Cu(111), we found similar cooperative effects of the inert fragments on several occasions, as schematically shown in Figure 12.

(a) During the butane formation step C1→D1, the activation barrier of 0.78 eV is lowered by 0.21 eV when the dmap and Cu(dmap) fragments exist around the adsorbed Et_2Zn. The presence of these dmap ligands prevents the migration of Et to the Cu surface and enables the formation of

butane with a lower activation barrier, explaining the advantage of using a copper metalorganic compound like $Cu(dmap)_2$ in ALD.

(b) The formation of the $Zn(dmap)_2$ by-product during ligand diffusion and re-ordering steps was eased by the presence of nearby Et groups (see F4 configuration). The E3→F4 reaction needs 0.1 – 0.2 eV less activation energy than E1→F2 and E3→F3. Although E1→F1 requires less activation energy than E3→F4, it faces a higher barrier in the next step. Moreover, E3→F4 completes formation of $Zn(dmap)_2$ in a single step, unlike the other reactions. This implies that the presence of nearby fragments not only reduces the activation barrier, but it may also speed up the formation of by-product.

(c) We found that butane formation on the bare Cu(111) surface needs an activation barrier of 0.99 eV, but that this process can be facilitated with the formation of the $Cu(Et)_2$ intermediate product from a Cu adatom (F4 → G2 → H2). Butane formation from $Cu(Et)_2$ needs 0.5 eV less activation compared to that without $Cu(Et)_2$ on a bare surface. This shows that local roughness due to newly deposited Cu adatoms also plays a cooperative role in the formation of by-products.

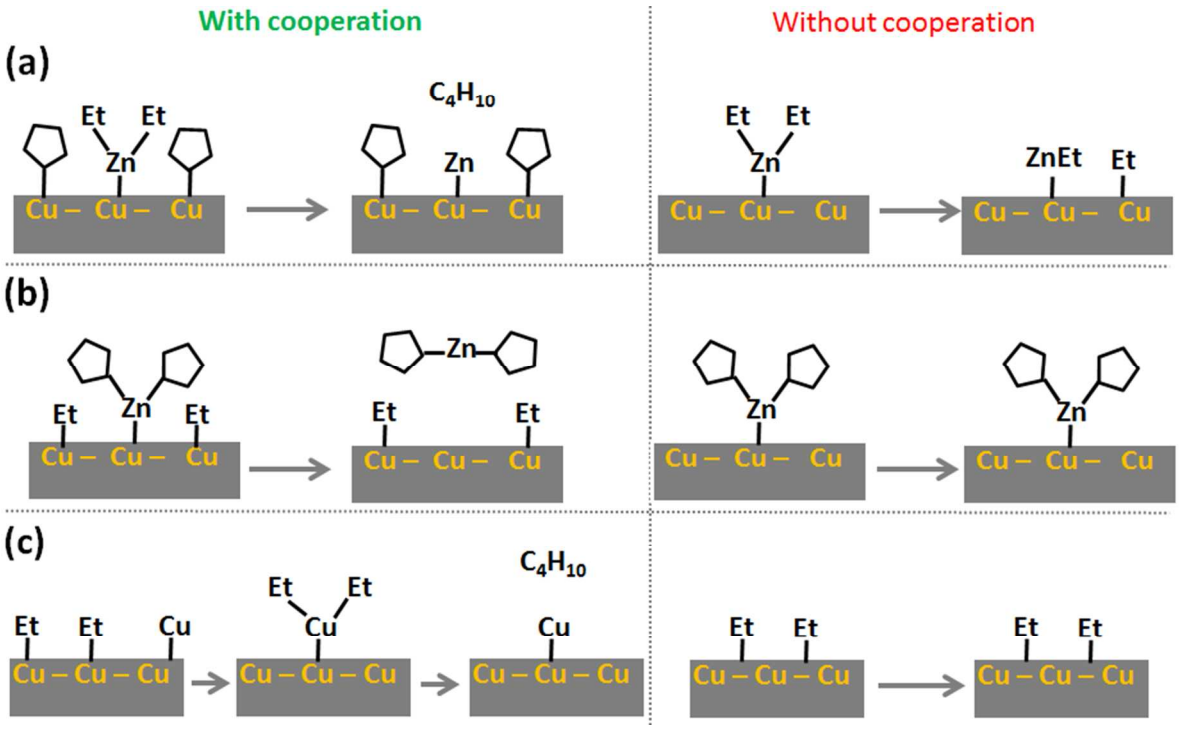

Figure 12. Schematic illustration of several cases of cooperative effects during the ALD of Cu from $Cu(dmap)_2$ and Et_2Zn. Pentagonal shapes represent the dmap ligand.

Overall, without the cooperative role of ligands and Cu adatoms, the reaction in Equation 1 would face higher activation barriers and need a higher ALD temperature. This strong dependence of activation energy on proximity of co-adsorbates must also be borne in mind when assessing the quality of our model and accuracy of computed activation energies. If we had modelled the reactions using a smaller cell, e.g. Cu(111) - (5 × 5) or if we had added extra ligands to the surface cell, making the surface more crowded, the activation barriers could have been slightly lower than what is reported in Table 1. However, the qualitative reaction mechanisms proposed in Figure 11 may not be affected.

5. Conclusion

Atomic layer deposition (ALD) is a promising method for depositing conformal and uniform thin films of copper for future electronic devices. However, the reaction mechanism and the surface chemistry of copper ALD have been unclear. In this work, we employ density functional theory to study the ALD reaction of copper dimethylamino-2-propoxide [$Cu(dmap)_2$] and diethylzinc [Et_2Zn] based on the seminal paper of Lee *et al.*[21], computing activation energies and reaction energies for a range of surface reactions.

We found that the chemisorbed $Cu(dmap)_2$ decomposes through breaking one or both Cu–O on Cu(111) during the $Cu(dmap)_2$ pulse. The surface saturates with rather immobile dmap and Cu(dmap) fragments, which prevents multilayer adsorption of $Cu(dmap)_2$ precursors, thus meeting the condition for ALD. The reaction of Et_2Zn with the dmap and Cu(dmap) fragments at the surface proceeds via two different reaction routes. The first route starts with butane formation from the adsorbed Et_2Zn molecule, aided through the cooperative role of dmap ligands on the surface. This is followed by the diffusion and reordering of dmap ligands around the Zn atom to form the $Zn(dmap)_2$ molecule, which finally desorbs. In the second case, the dmap ligands diffuse and re-order around the Zn atom. $Zn(dmap)_2$ is formed and desorbs in the presence of ethyl groups, which again lower the barriers for these reactions. Subsequently, butane formation is found not to occur on the bare Cu(111) surface. Instead, the intermediate reaction product $Cu(Et)_2$ is formed from the diffusion of adatom Cu on the surface and this facilitates butane formation and desorption.

In general, the butane formation and desorption steps are exothermic while the ligand diffusion and re-ordering steps are endothermic, which may result in residual dmap ligands blocking surface sites at the end of the Et_2Zn pulse, and in residual Zn being reduced and incorporated as

an impurity. It is found that the formation and desorption of Et_2Zn and $Zn(dmap)_2$ by-products are facilitated by the presence of nearby ligands (the 'cooperative effect').

In this transmetalation mechanism, the ALD growth rate is determined both by the saturating coverage of Et groups at the end of the Et_2Zn pulse (since each contributes one electron towards reduction of Cu) and by the saturating adsorption of $Cu(dmap)_2$ during the Cu pulse. Based on the rather slow rates of ligand diffusion that we computed, we suggest that saturation is reached before Et or dmap groups pack perfectly on the surface. We therefore estimate that Cu is deposited at approximately 0.18 Å/cycle, which agrees well with experiment.

We find that there is competition between alternative surface reactions, both leading to Cu deposition, and that which reaction mechanism is followed depends on the coverage of the ligands on the surface. We found that the cooperative role of ligands and Cu adatoms is an important factor that lowers activation barriers. The method that we used in this study and the ALD mechanisms that we obtained provide insight into the ALD of copper and other transition metals.

ASSOCIATED CONTENT

Supporting Information

The activation and reaction energies of depositing Cu from $Cu(dmap)_2$ and Et_2Zn through ALD. Structures of $Cu(dmap)_2$ decomposition on Cu(111) Surface. Reaction energy profiles and structures of butane formation on Cu(111) surface. This material is available free of charge via the Internet at http://pubs.acs.org.

AUTHOR INFORMATION

Corresponding Author

*Phone: +353 21 234 6392. E-mail: simon.elliott@tyndall.ie

Notes

The authors declare no competing financial interest.

ACKNOWLEDGEMENTS

We acknowledge support from Science Foundation Ireland (SFI) under the 'ALDesign' Project (grant number 09.IN1.I2628). We acknowledge the SFI and Higher Education Authority funded Irish Centre for High Performance Computing (ICHEC) for access and SFI funded computational resources at Tyndall National Institute. Y.M. thanks Dr. Gangotri Dey (George Washington University) for discussions.

REFERENCES

(1) Osada, T.; Godwin, M. International Technology Roadmap for Semiconductors http://www.itrs.net/.

(2) Rosenberg, R.; Edelstein, D. C.; Hu, C. K.; Rodbell, K. P. Copper Metallization for High Performance Silicon Technology. *Annu. Rev. Mater. Sci.* **2000**, *30*, 229–262.

(3) Shacham-Diamand, Y.; Inberg, A.; Sverdlov, Y.; Bogush, V.; Croitoru, N.; Moscovich, H.; Freeman, A. Electroless Processes for Micro- and Nanoelectronics. In *Electrochimica Acta*; 2003; Vol. 48, pp 2987–2996.

(4) Krisyuk, V.; Aloui, L.; Prud'homme, N.; Sysoev, S.; Senocq, F.; Samélor, D.; Vahlas, C. CVD of Pure Copper Films from Amidinate Precursor. *Electrochem. Solid-State Lett.* **2011**, *14* (3), D26–D29.

(5) Törndahl, T.; Ottosson, M.; Carlsson, J.-O. Growth of Copper Metal by Atomic Layer Deposition Using copper(I) Chloride, Water and Hydrogen as Precursors. *Thin Solid Films* **2004**, *458* (1-2), 129–136.

(6) Knisley, T. J.; Ariyasena, T. C.; Sajavaara, T.; Saly, M. J.; Winter, C. H. Low Temperature Growth of High Purity, Low Resistivity Copper Films by Atomic Layer Deposition. *Chem. Mater.* **2011**, *23* (20), 4417–4419.

(7) Coyle, J. P.; Dey, G.; Sirianni, E. R.; Kemell, M. L.; Yap, G. P. A.; Ritala, M.; Leskelä, M.; Elliott, S. D.; Barry, S. T. Deposition of Copper by Plasma-Enhanced Atomic Layer Deposition Using a Novel N-Heterocyclic Carbene Precursor. *Chem. Mater.* **2013**, *25* (7), 1132–1138.

(8) Hagen, D. J.; Povey, I.; Rushworth, S.; Wrench, J. S.; Keeney, L.; Schmidt, M.; Petkov, N.; Barry, S. T.; Coyle, J. P.; Pemble, M. E. Atomic Layer Deposition of Cu Using a Carbene-Stabilized Cu (I) Silylamide. *J. Mater. Chem. C* **2014**, 9205–9214.

(9) Kalutarage, L. C.; Clendenning, S. B.; Winter, C. H. Low-Temperature Atomic Layer Deposition of Copper Films Using Borane Dimethylamine as the Reducing Co-Reagent. *Chem. Mater.* **2014**, *26* (12), 3731–3738.

(10) George, S. M. Atomic Layer Deposition: An Overview. *Chem. Rev.* **2010**, *110* (1), 111–131.

(11) Profijt, H. B.; Potts, S. E.; van de Sanden, M. C. M.; Kessels, W. M. M. Plasma-Assisted Atomic Layer Deposition: Basics, Opportunities, and Challenges. *J. Vac. Sci. Technol. A Vacuum, Surfaces, Film.* **2011**, *29* (5), 50801–50826.

(12) Miikkulainen, V.; Leskelä, M.; Ritala, M.; Puurunen, R. L. Crystallinity of Inorganic Films Grown by Atomic Layer Deposition: Overview and General Trends. *J. Appl. Phys.* **2013**, *113* (2), 021301.

(13) Mårtensson, P.; Carlsson, J.-O. Atomic Layer Epitaxy of Copper on Tantalum. *Chem. Vap. Depos.* **1997**, *3* (1), 45–50.

(14) Niskanen, A.; Rahtu, A.; Sajavaara, T.; Arstila, K.; Ritala, M.; Leskelä, M. Radical-Enhanced Atomic Layer Deposition of Metallic Copper Thin Films. *J. Electrochem. Soc.* **2005**, *152* (1), G25–G28.

(15) Jezewski, C.; Lanford, W. A.; Wiegand, C. J.; Singh, J. P.; Wang, P.-I.; Senkevich, J. J.; Lu, T.-M. Inductively Coupled Hydrogen Plasma-Assisted Cu ALD on Metallic and Dielectric Surfaces. *J. Electrochem. Soc.* **2005**, *152* (2), C60–C64.

(16) Li, Z.; Rahtu, A.; Gordon, R. G. Atomic Layer Deposition of Ultrathin Copper Metal Films from a Liquid Copper(I) Amidinate Precursor. *J. Electrochem. Soc.* **2006**, *153* (11), C787–C794.

(17) Dai, M.; Kwon, J.; Halls, M. D.; Gordon, R. G.; Chabal, Y. J. Surface and Interface Processes during Atomic Layer Deposition of Copper on Silicon Oxide. *Langmuir* **2010**, *26* (6), 3911–3917.

(18) Gordon, P. G.; Kurek, A.; Barry, S. T. Trends in Copper Precursor Development for CVD and ALD Applications. *ECS J. Solid State Sci. Technol.* **2014**, *4* (1), N3188–N3197.

(19) Hagen, D. J.; Connolly, J.; Nagle, R.; Povey, I. M.; Rushworth, S.; Carolan, P.; Ma, P.; Pemble, M. E. Plasma Enhanced Atomic Layer Deposition of Copper: A Comparison of Precursors. *Surf. Coatings Technol.* **2013**, *230* (0), 3–12.

(20) Vidjayacoumar, B.; Emslie, D. J. H.; Clendenning, S. B.; Blackwell, J. M.; Britten, J. F.; Rheingold, A. Investigation of AlMe3, BEt3, and ZnEt2 as Co-Reagents for Low-Temperature Copper Metal ALD/Pulsed-CVD. *Chem. Mater.* **2010**, *22* (17), 4844–4853.

(21) Lee, B. H.; Hwang, J. K.; Nam, J. W.; Lee, S. U.; Kim, J. T.; Koo, S.-M.; Baunemann, A.; Fischer, R. a.; Sung, M. M. Low-Temperature Atomic Layer Deposition of Copper Metal Thin Films: Self-Limiting Surface Reaction of Copper Dimethylamino-2-Propoxide with Diethylzinc. *Angew. Chemie - Int. Ed.* **2009**, *48* (Spp 1119), 4536–4539.

(22) Hambrock, J.; Schröter, M. K.; Birkner, A.; Wöll, C.; Fischer, R. a. Nano-Brass: Bimetallic Copper/Zinc Colloids by a Nonaqueous Organometallic Route Using [Cu(OCH(Me)CH2NMe2)2] and Et 2Zn as Precursors. *Chem. Mater.* **2003**, *15* (22), 4217–4222.

(23) Vidjayacoumar, B.; Emslie, D. J. H.; Blackwell, J. M.; Clendenning, S. B.; Britten, J. F. Solution Reactions of a Bis(pyrrolylaldiminate)copper(II) Complex with Peralkyl Zinc, Aluminum, and Boron Reagents: Investigation of the Pathways Responsible for Copper Metal Deposition. *Chem. Mater.* **2010**, *22* (17), 4854–4866.

(24) Dey, G.; Wrench, J. S.; Hagen, D. J.; Keeney, L.; Elliott, S. D. Quantum Chemical and Solution Phase Evaluation of Metallocenes as Reducing Agents for the Prospective Atomic Layer Deposition of Copper. *Dalt. Trans.* **2015**, *44* (22), 10188–10199.

(25) Guo, Z.; Li, H.; Chen, Q.; Sang, L.; Yang, L.; Liu, Z.; Wang, X. Low-Temperature Atomic Layer Deposition of High Purity, Smooth, Low Resistivity Copper Films by Using Amidinate Precursor and Hydrogen Plasma. *Chem. Mater.* **2015**, *27* (17), 5988–5996.

(26) Elliott, S. D. Atomic-Scale Simulation of ALD Chemistry. *Semicond. Sci. Technol.* **2012**, *27* (7), 074008.

(27) Elliott, S. D.; Greer, J. C. Simulating the Atomic Layer Deposition of Alumina from First Principles. *J. Mater. Chem.* **2004**, *14* (21), 3246–3250.

(28) Nolan, M.; Elliott, S. D. Competing Mechanisms in Atomic Layer Deposition of Er2 O 3 versus la2O3 from Cyclopentadienyl Precursors. *Chem. Mater.* **2010**, *22* (1), 117–129.

(29) Shirazi, M.; Elliott, S. D. Multiple Proton Diffusion and Film Densification in Atomic Layer Deposition Modeled by Density Functional Theory. *Chem. Mater.* **2013**, *25* (6), 878–889.

(30) Dey, G.; Elliott, S. D. Mechanism for the Atomic Layer Deposition of Copper Using Diethylzinc as the Reducing Agent: A Density Functional Theory Study Using Gas-Phase Molecules as a Model. *J. Phys. Chem. A* **2012**, *116* (35), 8893–8901.

(31) Phung, Q. M.; Vancoillie, S.; Pourtois, G.; Swerts, J.; Pierloot, K.; Delabie, A. Atomic Layer Deposition of Ruthenium on a Titanium Nitride Surface: A Density Functional Theory Study. *J. Phys. Chem. C* **2013**, *117* (38), 19442–19453.

(32) Elliott, S. D.; Dey, G.; Maimaiti, Y.; Ablat, H.; Filatova, E. A.; Fomengia, G. N. Modeling Mechanism and Growth Reactions for New Nanofabrication Processes by Atomic Layer Deposition. *Adv. Mater.* **2015**, 5367–5380.

(33) Jiang, X.; Wang, H.; Qi, J.; Willis, B. G. In-Situ Spectroscopic Ellipsometry Study of Copper Selective-Area Atomic Layer Deposition on Palladium. *J. Vac. Sci. Technol. A Vacuum, Surfaces, Film.* **2014**, *32* (4), 041513.

(34) Minjauw, M. M.; Dendooven, J.; Capon, B.; Schaekers, M.; Detavernier, C. Atomic Layer Deposition of Ruthenium at 100 °C Using the RuO4-Precursor and H2. *J. Mater. Chem. C* **2015**, *3* (1), 132–137.

(35) Dey, G.; Elliott, S. Copper(I) Carbene Hydride Complexes Acting Both as Reducing Agent and Precursor for Cu ALD: A Study through Density Functional Theory. *Theor.*

Chem. Acc. **2013**, *133* (1), 1–7.

(36) Dey, G.; Elliott, S. D. Quantum Chemical Study of the Effect of Precursor Stereochemistry on Dissociative Chemisorption and Surface Redox Reactions During the Atomic Layer Deposition of the Transition Metal Copper. *J. Phys. Chem. C* **2015**, *119* (11), 5914–5927.

(37) Hu, X.; Schuster, J.; Schulz, S. E.; Gessner, T. Simulation of ALD Chemistry of (nBu3P)2Cu(acac) and Cu(acac)2 Precursors on Ta(110) Surface. *Microelectron. Eng.* **2015**, *137*, 23–31.

(38) Hu, X.; Schuster, J.; Schulz, S. E.; Gessner, T. Surface Chemistry of Copper Metal and Copper Oxide Atomic Layer Deposition from copper(II) Acetylacetonate: A Combined First-Principles and Reactive Molecular Dynamics Study. *Phys. Chem. Chem. Phys.* **2015**, *17* (40), 26892–26902.

(39) Ma, Q.; Guo, H.; Gordon, R. G.; Zaera, F. Surface Chemistry of Copper(I) Acetamidinates in Connection with Atomic Layer Deposition (ALD) Processes. *Chem. Mater.* **2011**, *23* (14), 3325–3334.

(40) Maimaiti, Y.; Nolan, M.; Elliott, S. D. Reduction Mechanisms of the CuO(111) Surface through Surface Oxygen Vacancy Formation and Hydrogen Adsorption. *Phys. Chem. Chem. Phys.* **2014**, *16*, 3036–3046.

(41) Maimaiti, Y.; Elliott, S. D. Precursor Adsorption on Copper Surfaces as the First Step during the Deposition of Copper: A Density Functional Study with van Der Waals Correction. *J. Phys. Chem. C* **2015**, *119* (17), 9375–9385.

(42) Maimaiti, Y. Computational Study of the Growth of Copper Thin Films by Atomic Layer Deposition, University College Cork, 2015.

(43) Elliott, S. D.; Scarel, G.; Wiemer, C.; Fanciulli, M.; Pavia, G. Ozone-Based Atomic Layer Deposition of Alumina from TMA: Growth, Morphology, and Reaction Mechanism. *Chem. Mater.* **2006**, *18* (16), 3764–3773.

(44) Weckman, T.; Laasonen, K. First Principles Study of the Atomic Layer Deposition of Alumina by TMA/H2O-Process. *Phys. Chem. Chem. Phys.* **2015**, *17* (1), 17322–17334.

(45) Kresse, G.; Hafner, J. Ab Initio Molecular-Dynamics Simulation of the Liquid-Metal-Amorphous-Semiconductor Transition in Germanium. *Phys Rev B Condens Matter* **1994**, *49* (20), 14251–14269.

(46) Kresse, G.; Furthmüller, J. Efficiency of Ab-Initio Total Energy Calculations for Metals and Semiconductors Using a Plane-Wave Basis Set. *Comput. Mater. Sci.* **1996**, *6* (1), 15–50.

(47) Blochl, P. E. Projector Augmented-Wave Method. *Phys. Rev. B* **1994**, *50* (24), 17953–17979.

(48) Perdew, J. P.; Burke, K.; Ernzerhof, M. Generalized Gradient Approximation Made Simple. *Phys. Rev. Lett.* **1996**, *77* (18), 3865–3868.

(49) Dion, M.; Rydberg, H.; Schroder, E.; Langreth, D. C.; Lundqvist, B. I. Van Der Waals

Density Functional for General Geometries. *Phys. Rev. Lett.* **2004**, *92* (24), 246401.

(50) Klimeš, J.; Michaelides, A. Perspective: Advances and Challenges in Treating van Der Waals Dispersion Forces in Density Functional Theory. *J. Chem. Phys.* **2012**, *137* (12), 120901–120912.

(51) Henkelman, G.; Uberuaga, B. P.; Jonsson, H. A Climbing Image Nudged Elastic Band Method for Finding Saddle Points and Minimum Energy Paths. *J. Chem. Phys.* **2000**, *113* (22), 9901–9904.

(52) Henkelman, G.; Jónsson, H. Improved Tangent Estimate in the Nudged Elastic Band Method for Finding Minimum Energy Paths and Saddle Points. *J. Chem. Phys.* **2000**, *113* (22), 9978.

(53) Shirazi, M.; Elliott, S. D. Cooperation between Adsorbates Accounts for the Activation of Atomic Layer Deposition Reactions. *Nanoscale* **2015**, *7* (14), 6311–6318.

(54) Vandalon, V.; Kessels, W. M. M. What Is Limiting Low-Temperature Atomic Layer Deposition of Al2O3? A Vibrational Sum-Frequency Generation Study. *Appl. Phys. Lett.* **2016**, *108* (1), 011607–011611.

(55) Liu, W.; Savara, A.; Ren, X.; Ludwig, W.; Dostert, K.-H.; Schauermann, S.; Tkatchenko, A.; Freund, H.-J.; Scheffler, M. Toward Low-Temperature Dehydrogenation Catalysis: Isophorone Adsorbed on Pd(111). *J. Phys. Chem. Lett.* **2012**, *3* (5), 582–586.

(56) Tillotson, M. J.; Brett, P. M.; Bennett, R. a.; Grau-Crespo, R. Adsorption of Organic Molecules at the TiO2(110) Surface: The Effect of van Der Waals Interactions. *Surf. Sci.* **2015**, *632*, 142–153.

Table of Contents Graphic